ACS APPLIED MATERIALS & INTERFACES

www.acsami.org

Research Article

Sodium Alginate Micelle-Encapsulating Zinc Phthalocyanine Dye-Sensitized Photoelectrochemical Biosensor with CdS as the Photoelectric Material for Hg^{2+} Detection

Xiaoyan Yang,* Mengjie Zhang, Zixuan Chen, Yuwei Bu, Xue Gao, Yongkun Sui, and Yueqin Yu*

Cite This: *ACS Appl. Mater. Interfaces* 2021, 13, 16828−16836

Read Online

ACCESS | Metrics & More | Article Recommendations | Supporting Information

ABSTRACT: A simple and selective photoelectrochemical (PEC) biosensor was constructed for Hg^{2+} detection based on zinc phthalocyanine (ZnPc) dye-sensitized CdS using alginate not only as a carrier but also as a binder. First, CdS as a photoactive material was in situ modified on the electrode surface using a rapid and simple electrodeposition to obtain an initial photocurrent signal. Second, ZnPc was loaded in the amphiphilic alginate micelle and then was coated onto the CdS film surface via alginate as the binder. The photocurrent was subsequently enhanced due to the favorable dye sensitization effect of ZnPc to CdS. Finally, the thymine-rich probe DNA was immobilized on the modified ITO surface via coupling reaction between the carbonyl groups of the amphiphilic polymer and the amino groups of the probe DNA. In the presence of Hg^{2+}, the thymine−Hg^{2+}−thymine (T−Hg^{2+}−T) structure was formed due to the specific bond of Hg^{2+} with thymine, resulting in the decrease of photocurrent due to the increase of steric hindrance on the modified electrode surface. The proposed PEC biosensor for Hg^{2+} detection possessed a wide linear range from 10 pM to 1.0 μM with a detection limit of 5.7 pM. This biosensor provides a promising platform for detecting other biomolecules of interest.

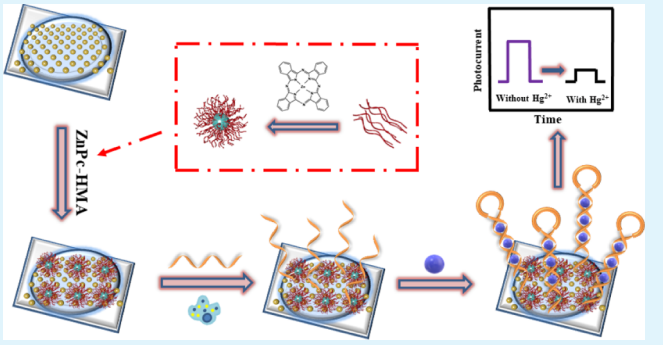

KEYWORDS: *photoelectrochemical, zinc phthalocyanine, alginate micelle, CdS, Hg^{2+}*

INTRODUCTION

Mercury ions (Hg^{2+}), as one of the most extremely toxic heavy metals, are a great threat to living things, especially human beings. Sensitive detection for mercury ions (Hg^{2+}) has always been an important issue in the field of environment and human health. The conventional methods for Hg^{2+} detection include colorimetry,[1] electrochemical method,[2−4] fluorescence,[5] chemiluminescence,[6] electrochemiluminescence,[7,8] and photoelectrochemical methods,[9,10] and so forth. Among these methods, photoelectrochemical (PEC) detection is a particularly promising analytical technique due to its inexpensive photoelectric devices and high sensitivity.[11] CdS, as a well-studied II−IV semiconductor, is commonly used in photoconductor devices, such as solar cells,[12,13] photoelectrochemical systems,[14] and electrochemiluminescence.[15] Recently, many approaches have been developed for PEC sensing to improve the photoelectric conversion efficiency and analytical performance. Dye sensitization is considered as a useful approach to improve the photon-to-electron conversion efficiency of photoelectrochemical systems, especially in the field of dye-sensitized solar cells which share a similar mechanism with a PEC biosensor.[16,17] Under light irradiation, the photo-induced electrons on the excited dye could be injected into the electrode via a semiconductor photocatalyst to produce current.[10] The zinc phthalocyanine (ZnPc) dye has a long excited state lifetime and an excellent charge transport property, which are beneficial to the transfer of electrons from the excited state of the dye molecules to the semiconductor conduction band.[18] More importantly, the energy band gap of ZnPc (~2.0 eV) is narrower than that of CdS (~2.38 eV), which could match well with the energy band gap of CdS.[19,20] Through combining the CdS and ZnPc, the absorption band of CdS could be broadened and the charge recombination could be inhibited, leading to an improved photoelectric conversion efficiency and the enhancement of photocurrent response for the sensing electrode. However, the attachment of the dye on the semiconductor surface requires at least an anchoring group located on the dye such as a carboxylate group, phosphonic acid group, or sulfonic group.[16] The synthesis of the anchoring group of the sensitizer dye

Received: January 5, 2021
Accepted: March 23, 2021
Published: March 31, 2021

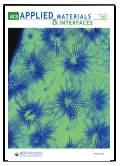

might require a strict means of preparation and treatment. Therefore, it is worth trying to find a convenient strategy for dye sensitization.

Alginate, a widely used biomaterial derived from brown seaweed, has many useful biomedical applications due to its excellent biocompatibility, low toxicity, relatively low cost, and suitableness for chemical modification.[21] Recently, it has been shown that alginate can be chosen as the ideal binder in lithium ion batteries and sodium ion batteries because of its abundant carboxylic groups, splendid adhesion, and good electrochemical stability.[22−24] Meanwhile, our previous work showed that a hydrophobic modified alginate (HMA), which used dodecyl glycidyl ether as a hydrophobic group, could form self-assembled micelles above the critical micelle concentration.[25] Also, these micelles could incorporate a hydrophobic drug and be triggered to release the drug in acidic medium or in the presence of α-L-fucosidase. It is well known that ZnPc has the characteristic of an intrinsically strong hydrophobicity; therefore, it could be noncovalently encapsulated into lipophilic interiors of the HMA micelles. However, the research on the sensitization of ZnPc loaded in the HMA micelles for use in the PEC biosensor remains poorly investigated despite HMA having the property of strong adhesion.

Herein, a PEC biosensor was proposed for highly sensitive and selective detection of Hg^{2+} via employing CdS as the photoactive material and ZnPc loaded in the HMA micelles as the sensitizer. As shown in Scheme 1, CdS was first in situ

Scheme 1. Schematic Illustration of a PEC Biosensor Based on CdS with ZnPc as the Sensitizer for Hg^{2+} Detection

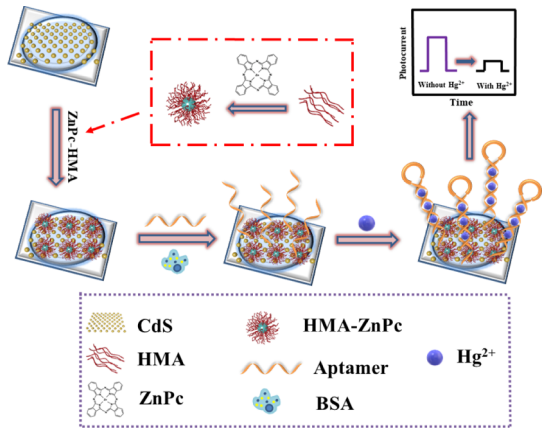

synthesized by the electrodeposition method, and HMA was utilized not only as the carrier to load ZnPc but also as the binder to adhere the encapsulated ZnPc onto the CdS film. The PEC response behavior demonstrated that the combination of ZnPc with CdS could greatly enhance the light absorption and the photocurrent response ability of the ZnPc/CdS due to the strong electronic coupling between the excited state of ZnPc and conduction band of CdS. Then, a single-stranded DNA (ssDNA) was immobilized on the modified indium tin oxide (ITO) surface via EDC coupling reaction between carbonyl groups of the amphiphilic polymer and the amino groups of the probe DNA. After that, bovine serum albumin (BSA) was coated onto the surface of the electrode for blocking the nonspecific sites. In the presence of Hg^{2+}, the structure transition from a flexible ssDNA to a rigid hairpin-shaped double-stranded DNA (dsDNA) was triggered by the target Hg^{2+} via a chemical coordination of T−Hg^{2+}−T, leading to a sharply decreased current response due to the increment of steric hindrance. As a result, the proposed PEC sensor for Hg^{2+} ions was simple and portable, demonstrating good performance with rapid response, high sensitivity, and good selectivity. It was successfully applied to the detection of Hg^{2+} in an aqueous system.

EXPERIMENTAL SECTION

Materials and Regents. Sodium alginate (SA) was obtained by Qingdao Bright Moon Seaweed Group Co., Ltd (China). The molecular weight and guluronate/mannuronate ratio of SA were 20 kDa and 1.5−3.0, respectively. Cadmium chloride ($CdCl_2$), zinc phthalocyanine (ZnPc), ascorbic acid (AA), sodium thiosulfate ($Na_2S_2O_3{\cdot}5H_2O$), 1-ethyl-3-(3-(dimethylamino) propyl) carbodiimide hydrochloride (EDC), *N*-hydroxysuccinimide (NHS), and BSA were purchased from Aladdin Chemistry Co. Ltd (China). Anhydrous ethanol, hydrochloric acid, mercury chloride ($HgCl_2$), ferric chloride ($FeCl_3$), copper sulfate ($CuSO_4$), and chlorine lead chemical ($PbCl_2$) were purchased from Shanghai Sinopac Chemical Reagent Co., LTD. All other reagents were of analytical grade and were used as received. All aqueous solutions were prepared with ultrapure water (18.2 MΩ cm), which was obtained from a Milli-Q water purification system. The oligonucleotides used in this work were ordered from Shenggong Bioengineering Co., Ltd. (Shanghai, China) with the following sequences: 5′−NH_2−TCA TGT TTG TTT GTT GGC CCC CCT TCT TTC TTA-3′

Apparatus. The morphology of the samples was characterized by scanning electron microscopy (SEM, JSM-6700F, Japan). Raman measurements were performed on an inVia Raman Microscope (Renishaw, England). UV−vis spectra were recorded using the UV−visible spectrophotometer (UH5300, Hitachi Manufacturing Co., Ltd.). Steady photoluminescence (PL) spectra were recorded on a PerkinElmer LS55 fluorescence spectrometer excited at 450 nm (PerkinElmer, U.K.). The size distribution was determined by dynamic light scattering (DLS) using the Zetasizer Nano-ZS90 instrument (Malvern Co., U.K.) with a laser light wavelength of 633 nm at a 90° scattering angle. Electrochemical impedance spectroscopy (EIS) was performed on CHI 660E electrochemical workstation (Shanghai Chenhua Apparatus Corporation, China) with a three-electrode system in 1.0 M KCl solution containing 5.0 mM $K_3[Fe(CN)_6]/K_4[Fe(CN)_6]$ (1:1) mixture as a redox probe and recorded in the frequency range of 0.1 Hz−10.0 kHz with an amplitude of 0.25 V. PEC measurements were performed with an in-house-built PEC system. The photocurrent was measured by the current−time curve experimental technique on a CHI832B electrochemical workstation (Chenhua Instruments, China). All experiments were performed at room temperature using a conventional three-electrode system with a modified ITO as the working electrode, a platinum wire as the auxiliary electrode, and a silver chloride electrode as the reference electrode.

Synthesis of ZnPc−HMA Micelle Solution. HMA was synthesized according to the previously reported method.[26,27] ZnPc was added into HMA solution (0.1 M PBS, pH = 7.4), followed by stirring at room temperature in dark for 24 h. After that, the free ZnPc which was not loaded into the HMA micelles was removed through the dialysis membrane tubing (MWCO 3500). Finally, the product was freeze−dried for 24 h. ZnPc−HMA micelle solution was obtained after the lyophilized product was dissolved in PBS solution.

Electrochemical Deposition of the CdS Film and the Modification of HMA−ZnPc. Electrodeposition is a widely used technique for electrode synthesis in various applications because of its low synthesis cost and easy scalability.[28] CdS films were prepared by a facile electrochemical deposition following the report with some modification.[29] Prior to the deposition of CdS, the ITO glass sheets were cleaned ultrasonically using ultrapure water, ethanol, and ultrapure water again, respectively. Subsequently, the CdS film was directly electrodeposited onto the ITO electrode from an aqueous bath containing $CdCl_2$ (0.1 M) and $Na_2S_2O_3$ (0.01 M). During the

https://doi.org/10.1021/acsami.1c00215
ACS Appl. Mater. Interfaces 2021, 13, 16828−16836

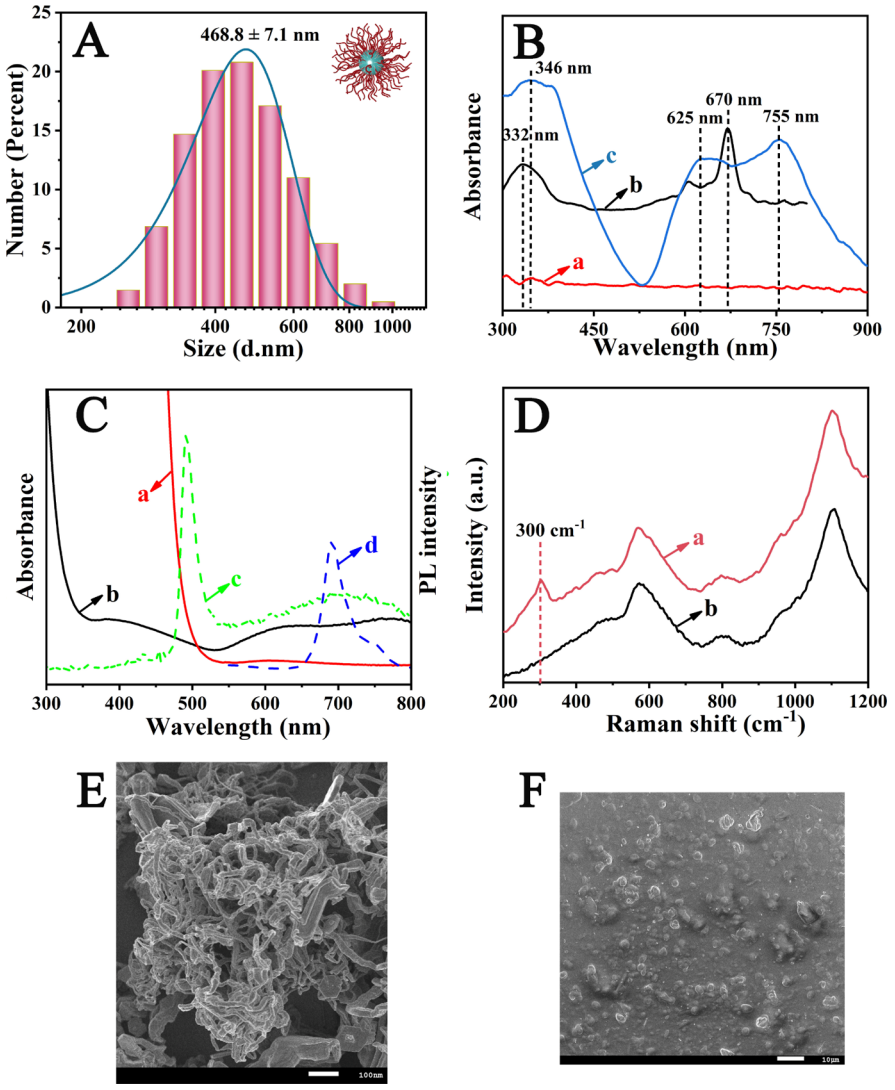

Figure 1. (A) Size analysis of HMA−ZnPc by dynamic light scattering. (B) UV−vis spectra of HMA (a), ZnPc (b), and HMA−ZnPc (c), (C) UV−vis spectra of CdS films (a) and of CdS/HMA−ZnPc (b) on the ITO substrate, PL of CdS films (c) on the ITO substrate and of ZnPc (d) in DMF. (D) Raman spectrum of CdS grown on ITO substrates by the electrochemical deposition method (curve a) and Raman spectrum of ITO substrates (curve b). The excitation wavelength was 532.0 nm. (E) SEM images of CdS films deposited on the ITO substrate in typical conditions. (F) SEM images of CdS/HMA−ZnPc.

electrodeposition, a constant potential of −1.0 V was applied to the ITO working electrode for 15 min. The resulting ITO/CdS electrode was thoroughly rinsed with ultrapure water and then dried under room temperature. Then, 10 μL of ZnPc−HMA solution was coated onto the surface of CdS and dried at room temperature.

Fabrication of the PEC Biosensor. An ssDNA was immobilized onto the ZnPc−HMA/CdS/ITO electrode via the classic EDC coupling reaction between carbonyl groups on the surface of the ZnPc−HMA micelles and the amino groups of the ssDNA. Specifically, the ZnPc−HMA micelle-modified electrode was activated with 20 μL PBS solution (0.01 M, pH 7.4) containing 0.8 M EDC solution and 0.2 M NHS solution for 1 h at room temperature, followed by rinsing with PBS solution (0.01 M, pH 7.4) to remove any excess EDC and NHS. Next, 10 μL of 10 μM ssDNA was dropped onto the electrode and was incubated at 4 °C for 12 h, and then the electrode was rinsed with PBS buffer to remove unbound ssDNA. The dosage of incubated ssDNA was in excess to ensure the maximum immobilization of the ssDNA on the electrode surface in order to increase the upper limit of detection for Hg^{2+}. After the electrode was incubated with 20 μL of 1% BSA for 1 h to block the unbound sites and then rinsing with PBS buffer, the electrode was employed as a PEC biosensor and was incubated with 20 μL of different concentrations of Hg^{2+} solutions for 1 h at 37 °C. Finally, the electrode was rinsed with PBS and prepared for the PEC test.

PEC Assay. PEC detection was performed at room temperature in PBS solution (0.01 M, pH 7.4) containing 0.1 M AA, which served as a sacrificial electron donor during measurement of the photocurrent. Blue light produced by a Xe lamp with a spectral range of above 425 nm was utilized as the excitation light, which was switched on and off every 10 s. The applied potential was 0.0 V.

RESULTS AND DISCUSSION

Characterization of the PEC Biosensor. The critical micelle concentration (CMC) of HMA was 0.05 g/L in PBS suffer (pH = 7.4) according to our previous work.[27] HMA was able to self-assemble into spherical micelles above the CMC, which could encapsulate the hydrophobic ZnPc. The size of HMA−ZnPc was determined by DLS. The mean hydrodynamic diameter of HMA−ZnPc was about 468.8 ± 7.1 nm (Figure 1A). UV−vis absorption spectra and photoluminescence spectra are used to investigate the optical property of CdS, ZnPc, and HMA. The UV−vis spectrum for the HMA

https://doi.org/10.1021/acsami.1c00215
ACS Appl. Mater. Interfaces 2021, 13, 16828−16836

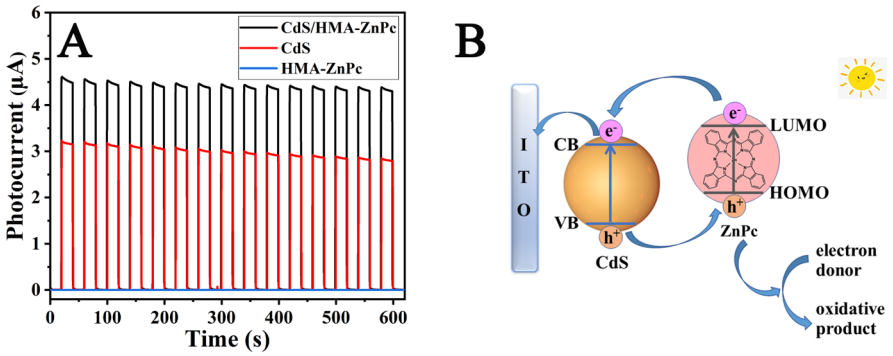

Figure 2. (A) Photocurrent response of CdS (red line), ZnPc–HMA (blue line), and CdS/ZnPc–HMA (black line) modified onto ITO electrodes. (B) Schematic mechanism of the operating PEC system.

displayed no remarkable absorption peak (Figure 1B, curve a). The UV–vis spectrum for ZnPc showed a strong band (Q band) at about 670 nm and a weak Soret (B) band at 332 nm (as shown in Figure 1B, curve b), which was consistent with the reported refs 20 and 30. The loading of ZnPc in the HMA micelles on the electrode could be estimated to be ~0.054 mg from the standard curve of ZnPc [Figure S1]. In comparison with free ZnPc, HMA–ZnPc exhibited red shift in both the Soret peak and Q band (Figure 1B, curve c). This revealed an increase in electronic density on porphyrin, which would facilitate the photoelectron injection process in photoelectrochemical systems.[17,31] As shown in Figure 1C, the absorption edge of CdS appeared at about 521 nm corresponding to its band gap of ~2.38 eV (curve a).[32,33] The absorption spectrum of CdS/HMA–ZnPc exhibited strong absorption bands in both the UV region and visible region, which were consistent with both CdS and ZnPc (curve b). The obvious absorption band in the red region indicated strong immobilization of the dye onto the CdS films. An obvious band appeared at ~500 nm, which was attributed to the spontaneous exciton transition at the CdS band gap (curve c).[34] In addition, a broad emission band from 550 to 800 nm was detected for the CdS film and arose from the recombination of trapped electrons/holes in some defect states.[35] Curve d showed the emission spectrum of ZnPc in DMF solution. The Raman spectrum of the CdS film on the ITO substrate revealed a typical band near 300 cm^{-1} assigned to the CdS longitudinal optical mode (Figure 1D, curve a).[36] Regardless of the dominant bands at higher frequencies around 600 and 1000 cm^{-1}, however, the background bands were also observed in the ITO substrate itself (Figure 1D, curve b). It could be obtained that the loading of CdS on the ITO electrode was ~1.13 mg, referring to Faraday's Law [$Q = nZF$, where Q is electric quantity, n is the amount of the substance, and F is the Faraday constant.]. The SEM images of CdS films are shown in Figure 1E, fibrous clusters of CdS deposited on the ITO substrate were exhibited, and the length of the CdS was about 200 μm. After the treatment of HMA–ZnPc, the surface became rougher and the CdS films were coated by HMA–ZnPc completely (Figure 1F).

Photoelectrochemical Measurements and PEC Mechanism. The photoelectrochemistry of the ZnPc–HMA-modified CdS electrode was studied in a conventional three-electrode configuration using a 425 nm Xe lamp as the light source. AA was used as an electron donor to promote charge separation as well as restrain the recombination of electron–hole pairs.[14] As shown in Figure 2A, in the absence of ZnPc–HMA, the photoelectrochemical intensity of the CdS film gradually degraded in the early stage (red line). This might be ascribed to the exfoliation of CdS from the electrode. At the same time, the HMA–ZnPc-modified CdS electrode produced a much higher and more stable photocurrent signal as compared with the CdS electrode, indicating that the transfer and separation efficiency of photogenerated electrons and holes was improved after sensitization of CdS with ZnPc–HMA (black line). Due to the presence of HMA as both the binder and dye carrier, the electrode exhibited a very good immobilization ability toward ZnPc. The photocurrent response was rather stable and did not show significant current decrease after several "on–off" cycles. This might be attributed to the strong bonding between active material and carboxyl groups on the binder surface to prevent active material loss to the electrolyte.[37−39] The photoelectrochemical behavior of ZnPc–HMA on the ITO electrode was also investigated, and a negligible PEC response could be seen, confirming that the photocurrent response comes from CdS rather than ZnPc–HMA (blue line). These results showed that the modified electrode could serve as a valid platform for photoelectrochemical assay of analytes.

The possible photoelectron transfer mechanism during PEC testing is schematically shown in Figure 2B. The conduction band (CB) and valence band (VB) energy levels of CdS, the highest occupied molecular orbital (HOMO), and lowest unoccupied molecular orbital (LUMO) of ZnPc were collected from the previous literatures.[14,18] An effective matching of energy was established between the LUMO of ZnPc and the CB of the CdS. Therefore, ZnPc adsorbed the photo under illumination, creating a charge-separated state and injecting the electron to the CB of CdS. The injected electron would be delivered to the ITO electrode, resulting in the enhanced photocurrent generation. Meanwhile, the holes would be transferred from the VB of CdS to ZnPc. AA, an efficient and nontoxic electron donor, scavenged the photogenerated holes of ZnPc and thus hindered electron–hole recombination processes, which largely increased the photovoltaic efficiency.[14]

Optimization of the Experimental Conditions. To obtain an acceptable signal response, a series of experiments conditions, such as the electrodeposition time of the CdS, the concentration of the ZnPc–HMA solution, and the incubation time for the DNA–Hg^{2+}, were optimized. CdS was in situ generated on the ITO electrode by the electrodeposition method. The electrodeposition time of the CdS on the ITO electrode is an important factor to influence the thickness of CdS films on the ITO electrode, which affects the photo-

https://doi.org/10.1021/acsami.1c00215
ACS Appl. Mater. Interfaces 2021, 13, 16828−16836

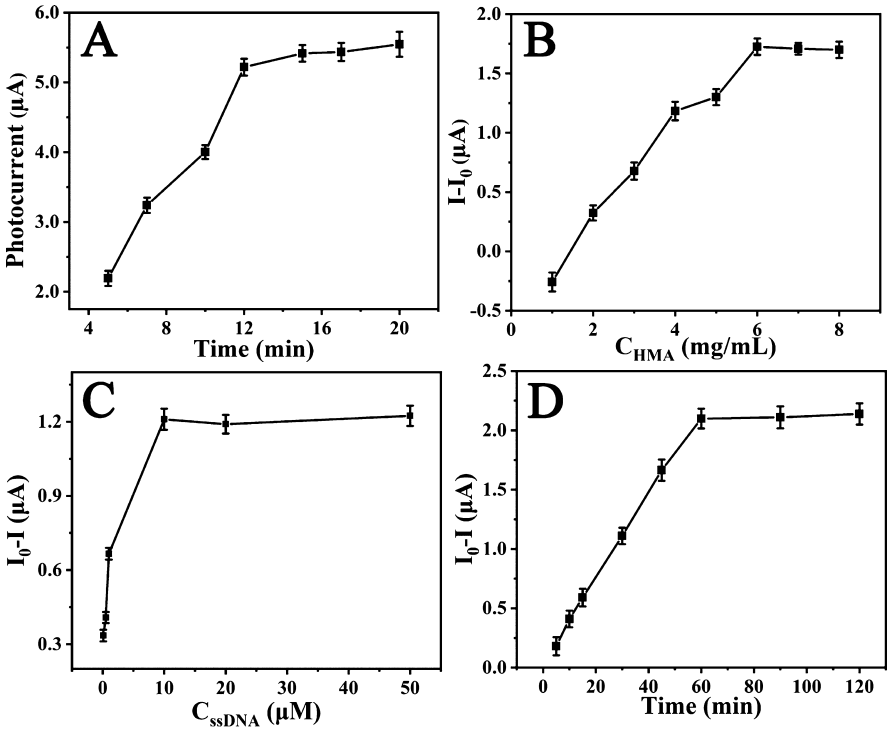

Figure 3. Effects of (A) electrodeposition time of CdS, (B) concentration of HMA solution, (C) concentration of ssDNA, and (D) incubation time of Hg^{2+} on the analytical performance of the aptasensing platform.

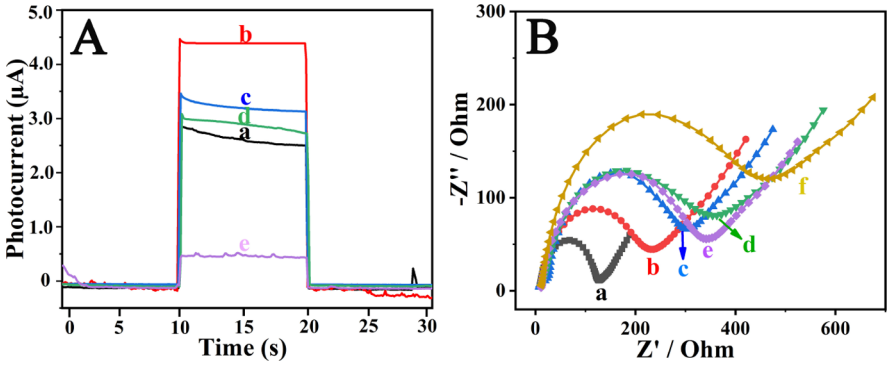

Figure 4. (A) Photocurrent intensity in 0.01 M PBS containing 0.10 M ascorbic acid of (a) CdS-modified ITO electrode, (b) modified with 6.0 mg/mL HMA−ZnPc, (c) hybridized with ssDNA, (d) blocked by 1% BSA, and (e) after target Hg^{2+} immobilization. (B) Nyquist diagrams of (a) bare ITO electrode, (b) CdS-modified ITO electrode, (c) modified with 6.0 mg/mL HMA−ZnPc, (d) hybridized with ssDNA, (e) blocked by 1% BSA, and (f) after target Hg^{2+} immobilization in PBS (0.1 M, pH 7.4) containing 0.1 M KCl and 5 mM $[Fe(CN)6]^{3-/4-}$ with the range of 0.1 Hz to 10.0 kHz.

electrochemical performance of the biosensor. As shown in Figure 3A, with the increasing of electrodeposition time, the photocurrent increased greatly from 5 to 15 min and then reached a plateau. The higher loading of CdS on the ITO electrode resulted in a better photocurrent response; thus, 15 min was selected as the optimum time for construction of the biosensor.

The thickness of the ZnPc−HMA film could be adjusted by the concentration of the ZnPc−HMA solution. To optimize the thickness of ZnPc−HMA film, different concentrations of ZnPc−HMA solution were used to prepare ITO/CdS/ZnPc−HMA. Figure 3B shows the relative photocurrent intensity ($I-I_0$) of the ITO/CdS/ZnPc−HMA electrodes prepared with different concentrations of ZnPc−HMA. It could be seen that the photocurrent increased as the concentration of the ZnPc−HMA increased from 1.0 to 6.0 mg/mL. However, as the ZnPc−HMA concentration increased further, the photocurrent intensity decreased slightly. It was inferred that excessive HMA increased the diffusion resistance to decrease the photocurrent intensity. Therefore, 6.0 mg/mL ZnPc−HMA was used for the following experiments.

The influence of the ssDNA concentration was also studied. As shown in Figure 3C, it could be seen that the PEC response gradually increased with the increase of the ssDNA concentration. After the concentration reached 10 μM, the PEC signal did not increase significantly. Thus, 10 μM ssDNA was selected to prepare the biosensor. Furthermore, it could be estimated that the loading of ZnPc−HMA with ssDNA was about 0.114 mg according to the optimization curve.

A DNA duplex with thymine−thymine (T−T) mismatch can specially capture Hg^{2+} to form a T−Hg−T complex, which is widely employed for Hg^{2+} sensing.[2,6] The effect of the

https://doi.org/10.1021/acsami.1c00215
ACS Appl. Mater. Interfaces 2021, 13, 16828−16836

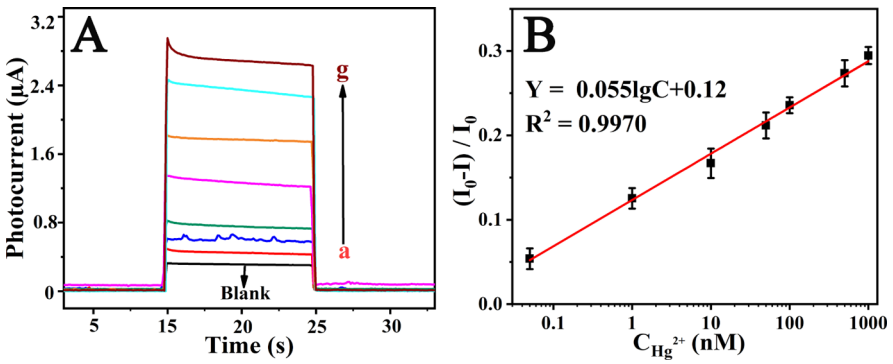

Figure 5. (A) Photocurrent responses of the PEC biosensor in 0.01 M PBS (pH = 7.4) containing 0.1 M AA with different concentrations of Hg^{2+}. (B) Corresponding calibration curves ($\Delta I = I - I_0$, with I_0 and I being the standard for the photocurrent of the aptasensor before and after incubation with Hg^{2+}, respectively). The error bars represent the standard deviations of three replicate determinations.

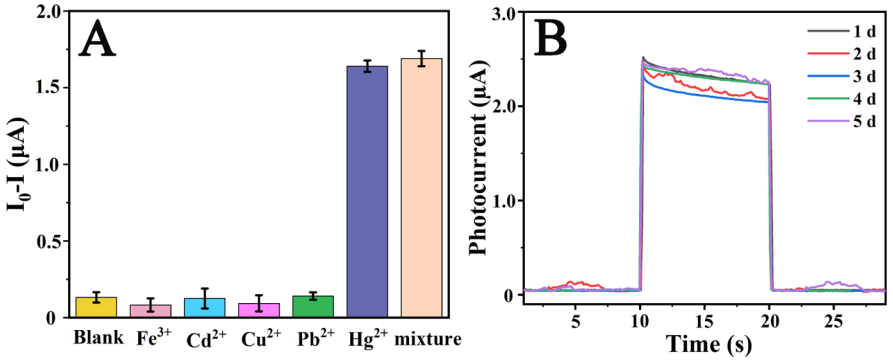

Figure 6. (A) Selectivity of the PEC aptasensor toward Hg^{2+} against Pb^{2+}, Cu^{2+}, Cd^{2+}, and Fe^{3+} (Note: The mixture contained the abovementioned analytes). (B) Stability of the PEC aptasensor under repeated light irradiation within 5 days.

incubation time for the DNA−Hg^{2+} on the photocurrent responses for 100 nM of Hg^{2+} was determined in the range of 5 to 120 min. As shown in Figure 3D, the relative photocurrent response increased along with the incubation time and reached a plateau at 60 min and did not show obvious changes at a longer time. Therefore, 60 min was chosen as the optimum time for the formation of the specific T−Hg^{2+}−T complex.

Analytical Performance of the PEC Biosensor. As shown in Figure 4A, the stepwise modification procedure of the prepared biosensor was performed by the PEC response. An apparent photocurrent signal (Figure 4A, curve a) was produced when CdS was electrochemical deposited on the ITO electrode. Moreover, the photocurrent signal was markedly enhanced after the decoration of ZnPc−HMA due to dye sensitization. Then, the photocurrent had slightly decreased after the immobilization of ssDNA and the blocking of BSA (Figure 4A, curve c and curve d). Finally, the PEC signal was further decreased owing to the formation of the stem rigid T−Hg^{2+}−T bonds and the consequent steric hindrance (curve e). To further manifest this viewpoint, the PEC response of the CdS/ITO electrode in PBS solution containing ssDNA and Hg^{2+} without HMA−ZnPc was measured (Figure S2). In the absence of HMA−ZnPc, no obvious difference could be seen between the CdS/ITO electrode in PBS solution containing ssDNA−$Hg^{2+}$and CdS/ITO electrode in PBS solution. These results implied that the T−Hg^{2+}−T complex with steric hindrance could not be immobilized on the electrode due to the lack of linker groups provided by HMA.

EIS was utilized to further verify the fabrication process of the proposed PEC biosensor. As shown in Figure 4B, the electron transfer resistance (R_{et}) of CdS/ITO (Figure 4B, curve b) increased compared with that of the bare ITO (Figure 4B, curve a), which indicated the successful deposition of CdS. When HMA−ZnPc was decorated onto the CdS/ITO (Figure 4B, curve c), the value of R_{et} increased significantly due to the poor conductivity of HMA. After ssDNA was immobilized on the HMA−ZnPc/CdS/ITO (Figure 4B, curve d), the value of R_{et} continued to increase because of the low conductivity of DNA sequences. The R_{et} value showed a slight change after the HMA−ZnPc/CdS/ITO electrode blocking with BSA (Figure 4B, curve e). After the modified electrode was incubated with Hg^{2+}, the R_{et} increased due to the increase of the steric hindrance of the sensing interface, implying that the ssDNA had hybridized with Hg^{2+} (Figure 4B, curve f).

PEC Detection of Hg^{2+}. On the basis of the abovementioned optimum conditions, the as-developed DNA/HMA−ZnPc/CdS/ITO electrode was applied to the quantitative determination of Hg^{2+}. As shown in Figure 5, the photocurrent response was found to be linearly decreasing with the increasing concentration of Hg^{2+} from 10 pM to 1.0 μM, with a detection limit of 5.7 pM. Compared with some recently reported methods [Table S1], the proposed PEC biosensor exhibited a comparable linear range and a lower detection limit, indicating that the present sensing strategy was a promising method for the Hg^{2+} detection.

Interferences and Application in Real Samples. In order to investigate the selectivity of the biosensor, various metal ions, such as Fe^{3+}, Cd^{2+}, Cu^{2+}, and Pb^{2+}, were selected

https://doi.org/10.1021/acsami.1c00215
ACS Appl. Mater. Interfaces 2021, 13, 16828−16836

for an interference test. As shown in Figure 6A, compared with the photocurrent response for the interferences, a sharp decrease of the photocurrent response for target (10 nM) was obtained, whereas the interfere solution remained nearly unchanged. The photoelectrochemical signal of a mixed metal ions solution (including Hg^{2+}) was almost identical to the Hg^{2+} solution, implying that the interfering substances had no obvious effect on the detection of Hg^{2+}. The result indicated that the proposed PEC biosensor possessed a satisfactory selectivity for Hg^{2+} detection as a result of the specific T−Hg^{2+}−T coordination chemistry. The stability of the PEC biosensor was also investigated. Figure 6B shows the signal response of the fabricated electrode in an experimental period of 5 days. No obvious change could be observed, indicating the good stability of the biosensor. The applicability of the PEC biosensor to detection of environmental samples was demonstrated by measuring the Hg^{2+} spiked into tap water. As shown in Table 1, the recovery values ranged from 96.0 to 100.7%, implying that the PEC biosensor had a high reliability for detecting Hg^{2+}.

Table 1. Recovery Studies of Hg^{2+}

sample number	added/nM	obtain/nM	recovery/%	RSD/%
1	0.1	0.096	96.0	3.7
2	1	1.007	100.7	4.6
3	10	9.65	96.5	4.1
4	50	50.09	100.2	3.5
5	400	402.40	100.6	2.9

CONCLUSIONS

In summary, the photoelectrochemical sensing performance of ZnPc-sensitized CdS for Hg^{2+} has been evaluated through the convenient micelle-encapsulating strategy. ZnPc−HMA played an important role in stabilizing and enhancing the photoelectrochemical intensity of CdS. As a result, the present dye-sensitized strategy exploited a simple and efficient approach to sensitively and specifically detect Hg^{2+}. Instead of the commonly used dye sensitization method, the present detection method is easily operated, cost-effective, and biocompatible, which makes it well suitable for practical applications.

ASSOCIATED CONTENT

Supporting Information

The Supporting Information is available free of charge at https://pubs.acs.org/doi/10.1021/acsami.1c00215.

UV−vis standard curve of ZnPc solution, PEC response of the CdS/ITO electrode in PBS solution (a) and of the CdS/ITO electrode in PBS solution containing ssDNA and Hg^{2+} without HMA−ZnPc (b), and comparison of various methods for the detection of Hg^{2+} (PDF)

AUTHOR INFORMATION

Corresponding Authors

Xiaoyan Yang − *Key Laboratory of Optic-electric Sensing and Analytical Chemistry for Life Science, MOE; Shandong Key Laboratory of Biochemical Analysis; Key Laboratory of Analytical Chemistry for Life Science in Universities of Shandong; College of Chemistry and Molecular Engineering, Qingdao University of Science and Technology, Qingdao 266042, PR China;* orcid.org/0000-0001-9701-8810; Phone: +86-532-84022681; Email: xyang@qust.edu.cn; Fax: +86-532-84022681

Yueqin Yu − *Key Laboratory of Optic-electric Sensing and Analytical Chemistry for Life Science, MOE; Shandong Key Laboratory of Biochemical Analysis; Key Laboratory of Analytical Chemistry for Life Science in Universities of Shandong; College of Chemistry and Molecular Engineering, Qingdao University of Science and Technology, Qingdao 266042, PR China;* orcid.org/0000-0003-0564-2179; Email: qustyu@163.com

Authors

Mengjie Zhang − *Key Laboratory of Optic-electric Sensing and Analytical Chemistry for Life Science, MOE; Shandong Key Laboratory of Biochemical Analysis; Key Laboratory of Analytical Chemistry for Life Science in Universities of Shandong; College of Chemistry and Molecular Engineering, Qingdao University of Science and Technology, Qingdao 266042, PR China*

Zixuan Chen − *Key Laboratory of Optic-electric Sensing and Analytical Chemistry for Life Science, MOE; Shandong Key Laboratory of Biochemical Analysis; Key Laboratory of Analytical Chemistry for Life Science in Universities of Shandong; College of Chemistry and Molecular Engineering, Qingdao University of Science and Technology, Qingdao 266042, PR China*

Yuwei Bu − *Key Laboratory of Optic-electric Sensing and Analytical Chemistry for Life Science, MOE; Shandong Key Laboratory of Biochemical Analysis; Key Laboratory of Analytical Chemistry for Life Science in Universities of Shandong; College of Chemistry and Molecular Engineering, Qingdao University of Science and Technology, Qingdao 266042, PR China*

Xue Gao − *Key Laboratory of Optic-electric Sensing and Analytical Chemistry for Life Science, MOE; Shandong Key Laboratory of Biochemical Analysis; Key Laboratory of Analytical Chemistry for Life Science in Universities of Shandong; College of Chemistry and Molecular Engineering, Qingdao University of Science and Technology, Qingdao 266042, PR China*

Yongkun Sui − *Key Laboratory of Optic-electric Sensing and Analytical Chemistry for Life Science, MOE; Shandong Key Laboratory of Biochemical Analysis; Key Laboratory of Analytical Chemistry for Life Science in Universities of Shandong; College of Chemistry and Molecular Engineering, Qingdao University of Science and Technology, Qingdao 266042, PR China*

Complete contact information is available at: https://pubs.acs.org/10.1021/acsami.1c00215

Notes

The authors declare no competing financial interest.

ACKNOWLEDGMENTS

We appreciated the finance supports from the Natural Science Foundation of Shandong Province of China (ZR2019MB051), Shandong Provincial Key Research and Development Program (2018GGX102001), and the Foundation of Key Laboratory of Optic-electric Sensing and Analytical Chemistry for Life Science (SATM201701).

REFERENCES

(1) Xue, X.; Wang, F.; Liu, X. One-Step, Room Temperature, Colorimetric Detection of Mercury (Hg^{2+}) Using DNA/Nanoparticle Conjugates. *J. Am. Chem. Soc.* **2008**, *130*, 3244−3245.

(2) Mor-Piperberg, G.; Tel-Vered, R.; Elbaz, J.; Willner, I. Nanoengineered Electrically Contacted Enzymes on DNA Scaffolds: Functional Assemblies for the Selective Analysis of Hg^{2+} Ions. *J. Am. Chem. Soc.* **2010**, *132*, 6878−6879.

(3) Zhang, Y.; Zeng, G. M.; Tang, L.; Chen, J.; Zhu, Y.; He, X. X.; He, Y. Electrochemical Sensor Based on Electrodeposited Graphene-Au Modified Electrode and NanoAu Carrier Amplified Signal Strategy for Attomolar Mercury Detection. *Anal. Chem.* **2015**, *87*, 989−996.

(4) Zhang, X.; Huang, C.; Jiang, Y.; Jiang, Y.; Shen, J.; Han, E. Structure-Switching Electrochemical Aptasensor for Single-Step and Specific Detection of Trace Mercury in Dairy Products. *J. Agric. Food Chem.* **2018**, *66*, 10106−10112.

(5) Zhang, Y.; Xiao, J.-Y.; Zhu, Y.; Tian, L.-J.; Wang, W.-K.; Zhu, T.-T.; Li, W.-W.; Yu, H.-Q. Fluorescence Sensor Based on Biosynthetic CdSe/CdS Quantum Dots and Liposome Carrier Signal Amplification for Mercury Detection. *Anal. Chem.* **2020**, *92*, 3990−3997.

(6) Cai, S.; Lao, K.; Lau, C.; Lu, J. "Turn-On" Chemiluminescence Sensor for the Highly Selective and Ultrasensitive Detection of Hg^{2+} Ions Based on Interstrand Cooperative Coordination and Catalytic Formation of Gold Nanoparticles. *Anal. Chem.* **2011**, *83*, 9702−9708.

(7) Lei, Y.-M.; Wen, R.-X.; Zhou, J.; Chai, Y.-Q.; Yuan, R.; Zhuo, Y. Silver Ions as Novel Coreaction Accelerator for Remarkably Enhanced Electrochemiluminescence in a PTCA−$S_2O_8^{2-}$ System and Its Application in an Ultrasensitive Assay for Mercury Ions. *Anal. Chem.* **2018**, *90*, 6851−6858.

(8) Yuan, T.; Liu, Z.; Hu, L.; Zhang, L.; Xu, G. Label-free Supersandwich Electrochemiluminescence Assay for Detection of Sub-nanomolar Hg^{2+}. *Chem. Commun.* **2011**, *47*, 11951−11953.

(9) Zhao, M.; Fan, G.-C.; Chen, J.-J.; Shi, J.-J.; Zhu, J.-J. Highly Sensitive and Selective Photoelectrochemical Biosensor for Hg^{2+} Detection Based on Dual Signal Amplification by Exciton Energy Transfer Coupled with Sensitization Effect. *Anal. Chem.* **2015**, *87*, 12340−12347.

(10) Zhang, B.; Meng, H.; Wang, X.; Chang, H.; Wei, W. Bio-dye Sensitized Detection of Hg^{2+} Based GO-ZnO-CdS Nanohybrids. *Sens. Actuators, B* **2017**, *253*, 495−501.

(11) Huang, L.; Yang, L.; Zhu, C.; Deng, H.; Liu, G.; Yuan, Y. Methylene Blue Sensitized Photoelectrochemical Biosensor with 3,4,9,10-Perylene Tetracarboxylic Acid Film as Photoelectric Material for Highly Sensitive Pb^{2+} Detection. *Sens. Actuators, B* **2018**, *274*, 458−463.

(12) Hwang, J.-Y.; Lee, S.-A.; Lee, Y. H.; Seok, S.-I. Improved Photovoltaic Response of Nanocrystalline CdS-Sensitized Solar Cells through Interface Control. *ACS Appl. Mater. Interfaces* **2010**, *2*, 1343−1348.

(13) Yu, X.-Y.; Liao, J.-Y.; Qiu, K.-Q.; Kuang, D.-B.; Su, C.-Y. Dynamic Study of Highly Efficient CdS/CdSe Quantum Dot-Sensitized Solar Cells Fabricated by Electrodeposition. *ACS Nano* **2011**, *5*, 9494−9500.

(14) Li, Y.-J.; Ma, M.-J.; Yin, G.; Kong, Y.; Zhu, J.-J. Phthalocyanine-Sensitized Graphene−CdS Nanocomposites: An Enhanced Photoelectrochemical Immunosensing Platform. *Chem.—Eur J.* **2013**, *19*, 4496−4505.

(15) Du, Y.; Li, X.; Ren, X.; Wang, H.; Wu, D.; Ma, H.; Fan, D.; Wei, Q. Signal-off Electrochemiluminescence Immunosensors Based on the Quenching Effect Between Curcumin-conjugated Au Nanoparticles Encapsulated in ZIF-8 and CdS-decorated TiO_2 Nanobelts for Insulin detection. *Analyst* **2020**, *145*, 1858−1864.

(16) Zhou, Y.; Shi, Y.; Wang, F.-B.; Xia, X.-H. Oriented Self-Assembled Monolayer of Zn(II)-Tetraphenylporphyrin on TiO_2 Electrode for Photoelectrochemical Analysis. *Anal. Chem.* **2019**, *91*, 2759−2767.

(17) Wang, H.; Li, M.; Zheng, Y.; Hu, T.; Chai, Y.; Yuan, R. An Ultrasensitive Photoelectrochemical Biosensor Based on $[Ru(dcbpy)_2dppz]^{2+}$/Rose Bengal Dyes Co-sensitized Fullerene for DNA Detection. *Biosens. Bioelectron.* **2018**, *120*, 71−76.

(18) Fan, Z.; Fan, L.; Shuang, S.; Dong, C. Highly Sensitive Photoelectrochemical Sensing of Bisphenol A Based on Zinc Phthalocyanine/TiO_2 Nanorod Arrays. *Talanta* **2018**, *189*, 16−23.

(19) Wang, L.; Gao, Z.; Li, Y.; She, H.; Huang, J.; Yu, B.; Wang, Q. Photosensitization of CdS by Acid red-94 Modified Alginate: Dual Ameliorative Effect upon Photocatalytic Hydrogen Evolution. *Appl. Surf. Sci.* **2019**, *492*, 598−606.

(20) Cheng, Y.; Memar, A.; Saunders, M.; Pan, J.; Liu, C.; Gale, J. D.; Demichelis, R.; Shen, P.; Jiang, S. Dye Functionalized Carbon Nanotubes for Photoelectrochemical Water Splitting−role of Inner Tubes. *J. Mater. Chem. A* **2016**, *4*, 2473−2483.

(21) Liu, M.; Song, X.; Wen, Y.; Zhu, J.-L.; Li, J. Injectable Thermoresponsive Hydrogel Formed by Alginate-g-Poly(N-isopropylacrylamide) That Releases Doxorubicin-Encapsulated Micelles as a Smart Drug Delivery System. *ACS Appl. Mater. Interfaces* **2017**, *9*, 35673−35682.

(22) Kovalenko, I.; Zdyrko, B.; Magasinski, A.; Hertzberg, B.; Milicev, Z.; Burtovyy, R.; Luzinov, I.; Yushin, G. A. Major Constituent of Brown Algae for Use in High-Capacity Li-Ion BatteriesA Major Constituent of Brown Algae for Use in High-Capacity Li-Ion Batteries. *Science* **2011**, *334*, 75−79.

(23) Gurunathan, P.; Ette, P. M.; Ramesha, K. Synthesis of Hierarchically Porous SnO_2 Microspheres and Performance Evaluation as Li-Ion Battery Anode by Using Different Binders. *ACS Appl. Mater. Interfaces* **2014**, *6*, 16556−16564.

(24) Ling, L.; Bai, Y.; Wang, Z.; Ni, Q.; Chen, G.; Zhou, Z.; Wu, C. Remarkable Effect of Sodium Alginate Aqueous Binder on Anatase TiO_2 as High-Performance Anode in Sodium Ion Batteries. *ACS Appl. Mater. Interfaces* **2018**, *10*, 5560−5568.

(25) Gao, X.; Yu, Z.; Liu, B.; Yang, J.; Yang, X.; Yu, Y. A Smart Drug Delivery System Responsive to pH/enzyme Stimuli Based on Hydrophobic Modified Sodium Alginate. *Eur. Polym. J.* **2020**, *133*, 109779.

(26) Wu, J.; Wu, Z.; Zhang, R.; Yuan, S.; Lu, Q.; Yu, Y. Synthesis and Micelle Properties of the Hydrophobic Modified Alginate. *Int. J. Polym. Mater. Polym. Biomater.* **2017**, *66*, 742−747.

(27) Wu, Z.; Wu, J.; Zhang, R.; Yuan, S.; Lu, Q.; Yu, Y. Colloid Properties of Hydrophobic Modified Alginate: Surface Tension, ζ-potential, Viscosity and Emulsification. *Carbohydr. Polym.* **2018**, *181*, 56−62.

(28) Govindaraju, G. V.; Wheeler, G. P.; Lee, D.; Choi, K.-S. Methods for Electrochemical Synthesis and Photoelectrochemical Characterization for Photoelectrodes. *Chem. Mater.* **2017**, *29*, 355−370.

(29) Li, G.; Wu, L.; Li, F.; Xu, P.; Zhang, D.; Li, H. Photoelectrocatalytic Degradation of Organic Pollutants via a CdS Quantum Dots Enhanced TiO_2 Nanotube Array Electrode under Visible Light Irradiation. *Nanoscale* **2013**, *5*, 2118−2125.

(30) Drozdek, S.; Szeremeta, J.; Lamch, L.; Nyk, M.; Samoc, M.; Wilk, K. A. Two-Photon Induced Fluorescence Energy Transfer in Polymeric Nanocapsules Containing $CdSe_xS_{1-x}$/ZnS Core/Shell Quantum Dots and Zinc(II) Phthalocyanine. *J. Phys. Chem. C* **2016**, *120*, 15460−15470.

(31) Gobeze, H. B.; Das, S. K.; D'Souza, F. Femtosecond Transient Absorption Study of Supramolecularly Assembled Metal Tetrapyrrole−TiO_2 Thin Films. *J. Phys. Chem. C* **2014**, *118*, 16660−16671.

(32) Choi, H.; Nicolaescu, R.; Paek, S.; Ko, J.; Kamat, P. V. Supersensitization of CdS Quantum Dots with a Near-Infrared Organic Dye: Toward the Design of Panchromatic Hybrid-Sensitized Solar Cells. *ACS Nano* **2011**, *5*, 9238−9245.

(33) Cooper, J. K.; Cao, J.; Zhang, J. Z. Exciton Dynamics of CdS Thin Films Produced by Chemical Bath Deposition and DC Pulse Sputtering. *ACS Appl. Mater. Interfaces* **2013**, *5*, 7544−7551.

(34) Zhai, T.; Fang, X.; Bando, Y.; Liao, Q.; Xu, X.; Zeng, H.; Ma, Y.; Yao, J.; Golberg, D. Morphology-Dependent Stimulated Emission and Field Emission of Ordered CdS Nanostructure Arrays. *ACS Nano* **2009**, *3*, 949−959.

https://doi.org/10.1021/acsami.1c00215
ACS Appl. Mater. Interfaces 2021, 13, 16828−16836

(35) Amelia, M.; Flamini, R.; Latterini, L. Recovery of CdS Nanocrystal Defects through Conjugation with Proteins. *Langmuir* **2010**, *26*, 10129−10134.
(36) Boone, B. E.; Shannon, C. Optical Properties of Ultrathin Electrodeposited CdS Films Probed by Resonance Raman Spectroscopy and Photoluminescence. *J. Phys. Chem.* **1996**, *100*, 9480−9484.
(37) Kumar, P. R.; Jung, Y. H.; Kim, D. K. High performance of MoS_2 microflowers with a water-based binder as an anode for Na-ion batteries. *RSC Adv.* **2015**, *5*, 79845−79851.
(38) Ryou, M.-H.; Hong, S.; Winter, M.; Lee, H.; Choi, J. W. Improved cycle lives of $LiMn_2O_4$ cathodes in lithium ion batteries by an alginate biopolymer from seaweed. *J. Mater. Chem. A* **2013**, *1*, 15224−15229.
(39) Xu, H.; Jiang, K.; Zhang, X.; Zhang, X.; Guo, S.; Zhou, H. Sodium Alginate Enabled Advanced Layered Manganese-Based Cathode for Sodium-Ion Batteries. *ACS Appl. Mater. Interfaces* **2019**, *11*, 26817−26823.

https://doi.org/10.1021/acsami.1c00215
ACS Appl. Mater. Interfaces 2021, 13, 16828−16836